GSA Data Repository Item 2006224
for Geology paper G22826 - Chadwick et al.
A volcano bursting at the seams: Inflation, faulting, and eruption at Sierra Negra Volcano, Galápagos

1. Notes about CGPS data processing and reference stations used during this study.

Ionospheric corrections and other CGPS data processing procedures used in this study are the same as used by Bartel et al. (2003).

Bartel, B.A., Hamburger, M.W., Meertens, C.M., Lowry, A.R., and Corpuz, E., 2003, Dynamics of active magmatic and hydrothermal systems at Taal volcano, Philippines, from continuous GPS measurements: Journal of Geophysical Research, v. 108, p. 2475, doi:10.1029/2002JB002194.

GALA was the closest IGNS GPS site to Sierra Negra, located at the Charles Darwin Research Station in Puerto Ayora on Santa Cruz island, until it died on 07-Nov-02. A temporary site GAL2 was in operation from 07-Jan-03 to 07-Mar-03, which was then replaced by a permanent replacement site renamed GLPS on 28-Mar-03. However, GLPS was down from 01-Sep-05 until after the 22-Oct-2005 eruption.

GV01 and GV02 are dual-frequency instruments; GV03, GV04, GV05, GV06 are single-frequency instruments.

GV01 is relative to GALA/GLPS until it failed on 01-Dec-04. GV02 is relative to GALA/GLPS until it failed on 10-Jun-05. The level of noise in the CGPS results increased after 10-Jun-05, because both local dual-frequency instruments were down. GV03 is relative to GV01 until 01-Dec-04, then relative to GLPS until 01-Sep-05. After 01-Sep-05, GV01, GV02, and GLPS were all down. Between 01-Sep-05 and 22-Oct-05, displacements at GV03 were extrapolated, based on the average rates between 11-Jul-05 and 01-Sep-05. GV04, GV05 and GV06 are relative to GV01 until 01-Jan-04, then relative to GLPS until 01-Sep-05, then relative to the extraplated-GV03 until 22-Oct-05.

Table DR1. Approximate positions of the CGPS stations at Sierra Negra volcano.

	GV01	GV02	GV03	GV04	GV05	GV06
Latitude (S)	00° 46.94’	00° 48.88’	00° 47.87’	00° 48.69’	00° 48.30’	00° 50.06’
Longitude (W)	91° 06.80’	91° 07.98’	91° 07.98’	91° 08.29’	91° 07.27’	91° 07.69’

2. CGPS displacement vectors shown in Figure 1b,c (in meters).

Table DR2. CGPS displacements in Figures 1b and 1c (in meters).

01-Apr-03 to 21-Oct-05 (excluding the 16-Apr-05 trapdoor faulting event)						
	GV01*	GV02†	GV03	GV04	GV05	GV06
North	0.065	0.220	0.744	0.494	0.552	-0.989
East	0.020	-0.075	-0.244	-0.389	0.354	0.290
Vertical	0.038	1.177	1.053	1.749	1.544	1.107

* GV01 to 01-Dec-04 only.
† GV02 to 10-Jun-05 only.

All displacements were calculated from CGPS daily positions calculated as 5-point averages.

3. CGPS displacement vectors shown in Figure 2 a, b, c (in meters).

Table DR3. CGPS displacements shown in Figure 2a (in meters).

12-Feb-04 to 27-Jan-05 (inflation only)						
	GV01*	GV02	GV03	GV04	GV05	GV06
North	0.065	0.220	0.744	0.494	0.552	-0.989
East	0.020	-0.075	-0.244	-0.389	0.354	0.290
Vertical	0.038	1.177	1.053	1.749	1.544	1.107

* GV01 to 01-Dec-04 only.

Table DR4. CGPS displacements shown in Figure 2b (in meters).

27-Jan-05 to 12-May-05 (inflation and faulting)						
	GV01	GV02	GV03	GV04	GV05	GV06
North		0.227	0.146	0.186	0.149	0.058
East		-0.038	-0.030	-0.086	0.079	0.271
Vertical		0.474	0.143	0.358	0.245	1.000

Table DR5. CGPS displacements shown in Figure 2c (in meters).

15-Apr-05 to 17-Apr-05 (faulting only)†						
	GV01	GV02	GV03	GV04	GV05	GV06
North		0.146	-0.019	0.078	0.042	0.253
East		-0.004	-0.003	-0.004	0.016	0.019
Vertical		0.066	-0.030	-0.006	-0.023	0.792

† Daily results processed by Gypsy.

4. Notes on the inflating sill model used in the paper.

The best-fit sill-model for the InSAR/CGPS uplift between 12-Feb-04 and 27-Jan-05 was determined in two steps. First, parameters of a horizontal sill with uniform opening were estimated to determine the depth of the sill, and it was found to be 2.2 km (see table below). In the second step we fixed the sill depth at 2.2 km and the sill orientation at N55°E (approximately along the major axis of the elliptically shaped caldera), expanded the sill length and width, and solved for variable opening, which resulted in up to 1.5 m of opening. The results are listed in the table below:

Table DR6. Parameters for the sill model.

	Depth (km)	Length (km)	Width (km)	Orientation	Opening (m)
Uniform opening	2.2	5.0	2.9	N70°E	1.1 m
Variable opening	2.2*	10.0*	6.0*	N55°E*	0 - 1.5 m

* Denotes parameters that were held fixed in the inversion calculation.

The results of the sill model inversion are shown in the figures below.

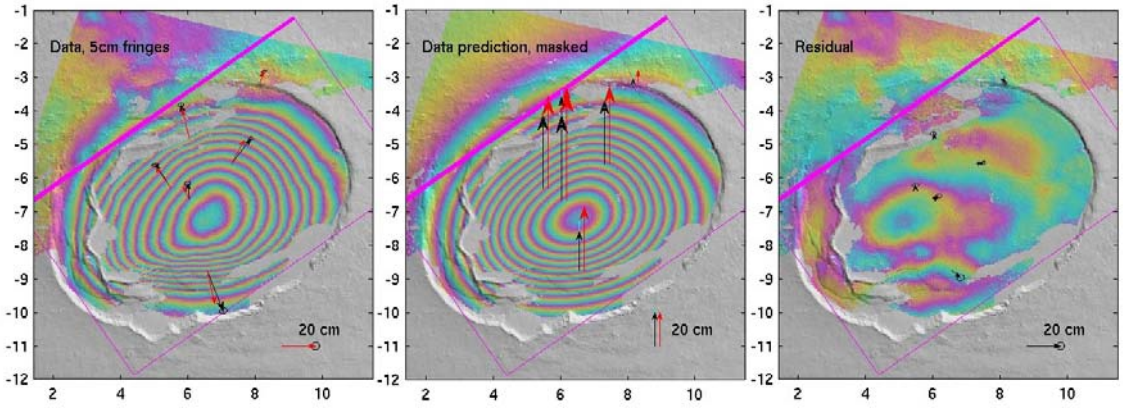

Figure DR1. InSAR data (left) in comparison with the sill model prediction (middle) and the residual (right) between the InSAR data and the model prediction. The InSAR data are displayed at 5 cm per color cycle, and represent the inflation between 12-Feb-04–27-Jan-05. The horizontal GPS data (black arrows) and model prediction (red) are shown on the left, the horizontal GPS residuals on the right, while the comparison of the vertical GPS measurements and model predictions are shown in the middle. Purple frame shows the outline of the 10 km x 6 km sill that was used in the estimation of the variable opening.

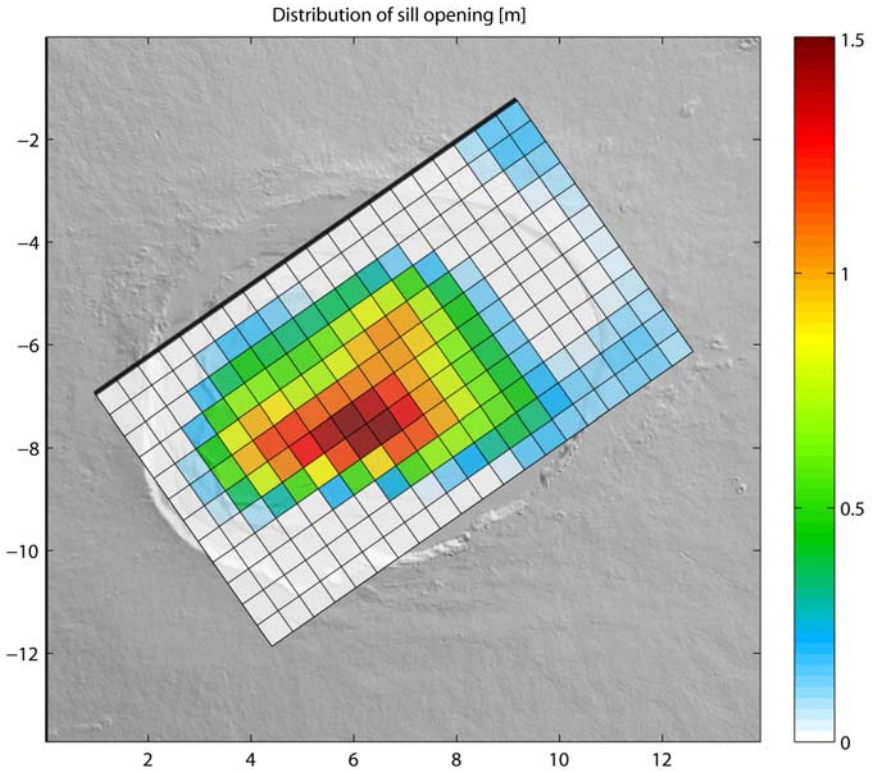

Figure DR2. Model results of variable opening of a sill at 2.2 km depth under Sierra Negra. The opening has a maximum of 1.5 m.

Note that in order to model the high fringe rate south of the uplift maximum, the sill opening has a very steep gradient south of the opening maximum, in comparison to other locations. It is interesting to speculate that there may be a barrier in the south, preventing the sill from propagating southward, resulting in this steep opening gradient. Perhaps this, in turn, results in high shear stresses in the sill roof at this location, promoting trapdoor faulting.

5. Notes on the fault modeling presented in the paper to fit displacements associated with the 16-Apr-2005 trapdoor faulting event.

We performed a joint inversion using both InSAR and CGPS data, as described in the paper. A non-linear optimization was carried out for the best-fit geometry of a single fault plane with 1) uniform dip-slip only, and 2) uniform slip with both dip- and strike-slip motion allowed. Then, we solved for spatially variable slip using fault parameters of the best fit fault #2.

The optimal fault geometry is almost exactly the same in the first two cases but the fit to CGPS station GV06 is greatly improved when strike-slip is included. The location, dimensions, and strike of the fault are constrained mostly by InSAR, whereas the dip, slip, and rake are constrained mainly by GPS. The best-fit model parameters are:

Table DR7. Best-fit parameters for fault models.

	Length (km)	Width (km)	Depth* (km)	Dip† (°)	Strike (°)	Strike slip (m)	Dip slip (m)	Rake (°)
Uniform-slip model (dip-slip only)	3.4	2.5	0.2	73	259	0.0	1.7	90
Uniform-slip model (dip-slip & strike-slip)	3.3	2.4	0.2	71	259	-0.6	1.5	111
Variable-slip model	6.0§	4.0§	0.0§	71§	259§	-0.9¶	1.9¶	97¶

* Depth is to upper edge of dipping fault plane.
† Dip is to the north (a reverse fault).
¶ These are maximum slip values and mean rake for the variable slip model
§ These parameters were held fixed in the inversion.

The resulting fault is a thrust that dips 71 degrees to the north. This differs from the trapdoor fault of Amelung et al. (2000) for the 1997-1998 event, which is a normal fault with a dip to the south (although we find the 1997-1998 data are better explained by a north-dipping fault - see later in this document). Therefore, the question here is: can we exclude all possible faults that dip to the south? To answer this question, we completed non-linear optimizations for different values of fault dip, and estimated optimal values for fault length, width, depth, strike, location, and slip in each case. We then investigated how the misfit changed as a function of fault dip and found that the weighted RMS misfit is 2 times higher for a fault dipping 71 degrees to the south, than for a fault dipping 71

degrees to the north. Faults that are nearly vertical, either dipping slightly to the south or to the north result in a smaller misfit, only about 1.2 times higher than the best fit fault, so it is harder to reject the possibility of a near vertical fault. This result does not depend on whether we estimate both dip-slip and strike-slip, or only dip-slip, components, nor on whether or not GPS station GV06 is included in the analysis.

Another way of looking at this problem is to estimate the model parameter confidence bounds from many model parameter optimizations using multiple realizations of the data covariance matrix. By doing this we find that the fault dip is statistically well constrained in the range of 68-74 degrees to the north (at a 95% confidence) and without strong trade-offs with other model parameters. The true fault-dip uncertainty is probably somewhat higher, as our confidence-bound calculation is based on only one possible fault model (i.e. single rectangular dislocation), and other fault-model scenarios (curving fault, multiple fault patches, etc.) would probably show a greater distribution of possible fault dips. However, based on our confidence interval calculation, we reject the possibility of a south dipping fault.

6. Notes on a revised trapdoor fault model that fits the 1997-8 InSAR data.

In the paper, we conclude that “the 1997-98 trapdoor event also occurred on a north dipping reverse fault, because a model similar to the one in Figure 2 can also fit the 1997-1998 InSAR data". This conclusion is based on the following:

The 1997-8 InSAR interferogram includes 13 months of inflation as well as the faulting, but in this case we cannot separate the two. However, we tried to do that using a method similar to the one we used in the paper for the 2005 faulting event. We removed

C x Uplift (12 Feb04 - 27 Jan 05)

from the 1997-8 interferogram, because the uplift pattern in 1992-7 and 1998-9 are very similar to the 2004-05 uplift pattern. The factor 'C' is estimated by trial and error. The resulting 'faulting only' signal for the 1997-8 event looks very similar to the 2005 event. The best fault dip for a simple (dip-slip only) fault is clearly dipping to the north, at 62°. A dip to the south has 2 times higher weighted RMS error. This result is also based on two major assumptions: (1) uplift can be removed, and (2) only dip-slip motion occurred. However, allowing for strike-slip motion also results in an optimal dip to the north. To deal with the uncertainty in removing the uplift, we also tried a combined inversion that allows for both faulting and sill opening. Here the optimal fault dip is closer to vertical, but still with a slight dip to the north. However, in this case, a range of fault dips can fit the data and there is not a significant difference in the weighted RMS error between solutions with fault dip of 75 degrees to the south to 40 degrees to the north. The reason is that here we invert for geometries of both a fault and a sill, and there are significant trade-offs between model parameters, most notably between fault dip and sill depth. For acceptable fault dips to the south the sill tends to be deep (~2.2 km), but for acceptable fault dips to the north it is shallower (~1.7-2.1 km).

Differences in the current modeling compared to the models of Amelung et al [2000] include: (1) one fault, instead of four, (2) Quadtree InSAR data sub-sampling, and (3) a full data covariance matrix.

7. Notes on daily vs. instantaneous (kinematic) displacements at GV06 during the 16-Apr-2005 trapdoor faulting event.

The daily and instantaneous displacements at GV06 associated with the 16-Apr-2005 trapdoor faulting event are similar.

Table DR8. Kinematic vs. daily CGPS displacements from the 16-Apr-05 faulting event.

	North displacement (m)	East displacement (m)	Vertical displacement (m)
Kinematic solution (10 sec)*	0.330	0.142	0.839
Kinematic solution (1 min)†	0.308	0.158	0.808
Daily solution (Bernese)†	0.240	0.195	0.788
Daily solution (Gypsy)†¶	0.253	0.193	0.792

* Displacements from single points (10 second epochs) before and after the earthquake (no averaging). These results are like the ones shown in the inset to Figure 1f in the paper.
† Displacements from 5-point averages before and after the earthquake.
¶ These are the results used in the fault modeling.

Therefore, it does not appear that there was significant post-seismic fault displacement following the earthquake. The differences between the kinematic and daily solutions are probably due to the relative inaccuracy of the kinematic solutions, rather than post-seismic displacement.